Vol. 10 No. 4 Oktober 2003

Jurnal TEKNIK SIPIL

Bonding at Particle Contacts

Suyud R. Karyasuparta

Abstract

This investigation deals with the behavior of cohesive bonding at particle contacts in soil. Direct measurement of cohesive strength at sliding contacts between particles of soil has not been accomplished. An indirect method is used in this study to estimate average contact cohesion from measurement of total strength of soil specimens.

Two types of materials were tested; Ottawa sand and crushed quartz, with two different relative densities, 25 and 75 percents; each material was tested with four different cement contents, 0, 2, 4, and 6 percents of cement by weight. Adding cement was to create controlled cohesion to the contacts between particles.

The results of 118 Consolidated Drained Triaxial compression tests on sand-cement specimens were analyzed, and the model by Hardin (1985) was used to isolate cohesive and frictional bonding in cohesive materials. This model considers two basic mechanism of strength of soils, by considering bonding at particle contacts and kinematics of particle movement within an element of deforming soil.

The result shows that the dimensionless contact cohesion is linearly related to cement content for sand with relative density 25 percent, and is nonlinear for sand with relative density 75 percent. Dimensionless contact cohesion decreases with increasing relative density for cement content 2 and 4 percents, but it increases with increasing relative density for 6 percent cement content. Dimensionless contact cohesion is larger in rounded material compared with in angular material.

Keywords: *cohesive bonding, particle contacts, sliding contacts, contact cohesion.*

Abstrak

Penelitian ini adalah mengenai perilaku dari ikatan kohesif pada kontak antar butir tanah. Pengukuran langsung kohesi pada bidang geser kontak antara butir-butir tanah, belum pernah dilakukan. Suatu cara tidak langsung dipakai dalam studi ini, untuk memprakirakan kohesi kontak (pada bidang geser antara 2 butir) rata-rata, dari pengukuran tegangan-tegangan total pada benda uji tanah.

Dua jenis material pasir diuji; yaitu pasir Ottawa dan crushed quatz (quartz tumbuk), dengan 2 nilai relative density yaitu 25% dan 75%; tiap material diuji dengan 4 kadar semen yang berbeda yaitu 0%, 2%, 4% dan 6% berat semen. Penambahan semen pada pasir tersebut, adalah untuk menciptakan kohesi yang dapat diatur, pada bidang kontak.

Hasil uji Consolidated Drained Tiaxial compression *pada 118 benda uji pasir bersemen diatas, dianalisis, dan sebuah model dari Hardin (1985), dipakai untuk mengisolasi ikatan kohesi dan ikatan geser pada material kohesif. Model tersebut memperhatikan dua mekanisme dasar dari kekuatan tanah, dengan memperhatikan ikatan pada kontak antara butir dan kinematik dari pergerakan partikel dalam sebuah elemen dari tanah yang berdeformasi.*

Hasilnya memperlihatkan bahwa kohesi kontak tak berdimensi berhubungan linier terhadap kadar semen, untuk pasir dengan relative density *25%, dan tidak linier untuk pasir dengan* relative density *75%. Kohesi kontak tak berdimensi berkurang dengan bertambahnya* relative density, *untuk kadar semen 2 dan 4%, tetapi bertambah besar dengan naiknya* relative density, *untuk kadar semen 6%. Kontak kohesi tak berdimensi lebih besar pada pasir yang* rounded *dibanding dengan pada pasir yang angular.*

Kata-kata kunci: *ikatan kohesif, kontak antar butir-butir tanah, bidang geser kontak antar butir-butir tanah, kohesi kontak.*

1) Staf Pengajar Departemen Teknik Sipil, Fakultas Teknik Sipil dan Perencanaan, Institut Teknologi Bandung.

Catatan : Usulan makalah dikirimkan pada 31 Oktober 2003 dan dinilai oleh peer reviewer pada tanggal 17 Nopember 2003 – 19 Januari 2004. Revisi penulisan dilakukan antara tanggal 20 Nopember 2003 hingga 28 Januari 2004.

1. Introduction

Cohesive bonding is said to exist at a contact between two soil particles when the contact has tensile strength, or when the contact can resist a shearing force in the absence of a normal contact force. Direct measurement of the cohesive strength at contacts in a soil sample has not been accomplished. Thus, indirect methods are used to estimate average contact cohesion from measurement of the total strength of soil specimens. This requires a model for soil strength that accounts for existing strength components (friction, cohesion, dilation, etc.). The model is used to isolate the cohesion component, and to compute the magnitude of average contact cohesion c_μ, or some parameter related to c_μ, from measured total strength.

This investigation deals with the behavior of cohesive bonding at particle contacts in soil. The results of 118 drained triaxial compression tests on sand-cement specimens were analyzed, and the model by Hardin (1985) was used to isolate cohesive and frictional bonding in cohesive materials. This model considers the two basic mechanism of strength of soils, by considering bonding at particle contacts and the kinematics of particle movement within an element of deforming soil.

The study required many samples with varying amount of cohesion. The amounts of cohesive bonding in natural cohesive soil cannot be controlled. A convenient means of controlling cohesion is to test artificially cemented soils. The choice was made to test sand specimens with varying amounts of Portland cement. Sand is cohesion less material but cohesion is produced by the presence of cement in the sand.

Cohesion in sand-cement depends on the properties of sand particles and on the properties of the cement. Thus the cohesion of sand-cement specimens vary with particle mineralogy, grain size distribution, shape and hardness of particles, grain arrangements and density, cement content, curing time, etc. The results of this study indicate that the mineral friction angle ϕ_μ is about the same for cemented and uncemented sands.

Two types of materials were tested; Ottawa sand and crushed quartz, with two different relative densities, D_r = 25 and 75 percents; each material was tested with four different Portland cement contents, 0, 2, 4, and 6 percents of cement by weight. Consolidated Drained triaxial compression tests were carried out on the specimens in order to define the strength in terms of effective stress. Drained tests were also used in order to determine the volumetric strain behavior which is needed for application of Hardin's model.

The cohesion parameters of the Hardin and Schmertmann models have been compared. The magnitude of contact cohesion indicated by the two theories shows a high degree correlation.

2. Cohesion

2.1 Definition of true cohesion

The term cohesion as used in soil mechanics can be confusing. The cohesion that is measured by extending the Mohr-Coulomb failure envelope to normal stress $\sigma' = 0$, is not true cohesion because it includes the effects of dilation.

True cohesion is shear resistance which is mobilized between two adjacent particles which stick to each other without the existence of normal pressure; it is the force that arises within the particles themselves (Lambe, T. W. 1960). The existence of tensile or shear strength without the necessity of the existence of effective stress in the soil skeleton or on the failure plane can be taken as evidence of a true cohesion (Mitchell, J. K. 1976). It is the true cohesion that is the object of this study.

True cohesion is defined by considering the shear and normal forces, T_i and N_i, at a single sliding contact as shown in **Figure 2.1.**

The contact shearing resistance T_i will depend on the normal contact force N_i and the relationship may be expressed by the equation

$$T_i = C_{\mu i} + N_i \tan \phi_{\mu i} \qquad (2.1)$$

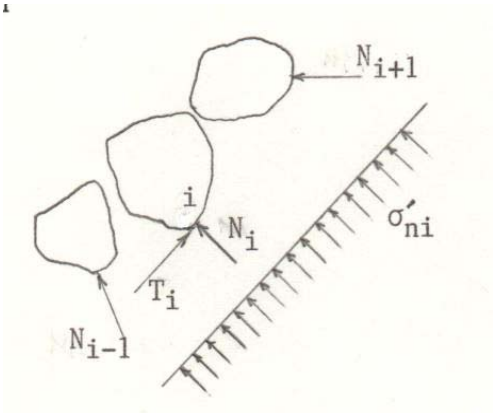

Figure 2.1 The shear and normal forces, T_i and N_i at a single sliding contact

where $C_{\mu i}$ is the contact cohesion force and $\phi_{\mu i}$ is the angle of mineral friction at contact i.

It should be noted that the relationship between T_i and N_i may be nonlinear in which case $\phi_{\mu i}$ is a function of N_i.

The orientation of contact i is defined by the direction cosines l_i , m_i , and n_i between N_i and the directions of the major, intermediate, and minor principal stresses σ_1' , σ_2' and σ_3' respectively, where σ_1' , σ_2' , and σ_3' are stresses in an element containing many particles. The stress σ'_{ni} in **Figure 2.1** normal to the contact plane at contact i is given by

$$\sigma'_{ni} = \sigma'_1 l_i^2 + \sigma'_2 m_i^2 + \sigma'_3 n_i^2 \qquad (2.2)$$

The normal contact force N_i is produced by the normal contact stress σ'_{ni} acting on an area A_i associated with sliding contact i where

$$A_i = \frac{N_i}{\sigma'_{ni}} \qquad (2.3)$$

The area A_i is also associated with the contact cohesion force $C_{\mu i}$ such that the unit contacts cohesion $c_{\mu i}$ is given by

$$c_{\mu i} = \frac{C_{\mu i}}{A_i} \qquad (2.4)$$

where $c_{\mu i}$ is the true cohesion at sliding contact i. The average of all $c_{\mu i}$ for all sliding contacts in an element of soil is the true cohesion c_μ for the soil.

2.2 Definition of bonding obliquity angle

The bonding obliquity angle ϕ_{0i} at sliding contact i in **Figure 2.1** is defined by

$$\tan \phi_{0i} = \frac{T_i}{N_i} \qquad (2.5)$$

Substituting **Equation 2.1** for T_i in **Equation 2.5** gives

$$\tan \phi_{0i} = \tan \phi_\mu + \frac{C_{\mu i}}{N_i} \qquad (2.6)$$

Substituting **Equation 2.3** into **Equation 2.4** and dividing by σ'_{ni} gives $c_{\mu i}/\sigma'_{ni} = C_{\mu i}/N_i$ which can be substituted into **Equation 2.6** resulting in

$$\tan \phi_{0i} = \tan \phi_{\mu i} + \frac{c_{\mu i}}{\sigma'_{ni}} \qquad (2.7)$$

Using average values of σ_μ, c_μ, and σ'_n for all sliding contacts in an element of soil, it is assumed that

$$\tan \phi_o = \tan \phi_\mu + \frac{c_\mu}{\sigma'_n} \qquad (2.8)$$

where ϕ_o is the bonding obliquity angle for an element of soil. [Note: using (average $c_{\mu i}/\sigma'_{ni}$) = (average $c_{\mu i}$ / average σ'_{ni}) is approximate but is the only practical way to proceed without assuming distributions for $c_{\mu i}$ and orientations of sliding contacts].

Finally, multiplying numerator and denominator of c_μ/σ'_n in **Equation 2.8** by atmospheric pressure p_a and substituting

$$C_b = \frac{c_\mu}{p_a} \qquad (2.9)$$

where C_b = average dimensionless contact cohesion, gives

$$\tan \phi_o = \tan \phi_\mu + C_b \left\{ \frac{p_a}{\sigma'_n} \right\} \qquad (2.10)$$

The stress σ'_n in **Equations 2.8** and **2.10** is the mean value of σ'_{ni} , i.e. the average effective stress normal to sliding contacts in an element of soil. Based on an analysis of the orientations of sliding contacts in an

$$\sigma'_n = \tfrac{1}{2}\left[(0.8 - 0.65\sin\phi_o)\sigma'_1 + (1.2 + 0.65\sin\phi_o)\sigma'_3\right] \qquad (2.11)$$

element of soil, Hardin (1985) recommends using the following :

2.3 Schmertmann's cohesion parameter

In 1960, Schmertmann and Osterberg developed the IDS curvehopping technique to separate strength into two components; one component I_ε that is independent of effective stress and the second component D_ε that depends on effective stress.

$$\tau_\varepsilon = I_\varepsilon + D_\varepsilon \qquad (2.12)$$

Furthermore, he isolated these components at various values of strain ε (indicated by the subscript ε on τ, I and D). By analysis of the I_ε values, Schmertmann obtains a parameter I_b which analysis of Schmertmann's results shows that I_b is approximately equal to c_μ ($I_b \approx c_\mu$ for sand-cement with relative density D_r = 25 percent, and $I_b = 0.75 c_\mu$ for sand-cement with D_r = 75 percent).

3. Strength Model

The strength model by Hardin (1985) is formulated in

terms of the bonding obliquity angle ϕ_o and the maximum rate of dilation d_{max} (defined below). Using this model the bonding obliquity angle for a soil specimen can be determined from the results of a drained triaxial compression test with volume change measurements. Values of ϕ_o determined in this way can be used with **Equations 2.10** and **2.11** to find values of $C_b = c_\mu / p_a$ and ϕ_μ

For triaxial compression, the strength model is given by:

$$R_{max} = K_{cv} + (2K_{min} - K_{cv})d_{max} \quad (3.1)$$

where R_{max} is the maximum principal stress ratio at the peak = $(\sigma_1' / \sigma_3')_{max}$; K_{cv} is the critical state energy transmission ratio which is equal to the principal stress ratio at the critical state,

$K_{cv} = R_{cv} = (\sigma_1' / \sigma_3')_{cv}$ and K_{min} is the minimum possible value of energy transmission ratio; and d_{max} is the maximum rate of dilation.

A plot of the theoretical relationships between R_{max} and D_{max} for various values of ϕ_o is shown in **Figure 3.1** Knowing values of R_{max} and D_{max}, values of ϕ_o can be determined graphically from **Figure 3.1.**

The critical state energy transmission ratio K_{cv} is related to the critical state angle of shearing resistance ϕ_{cv} by the equation

$$K_{cv} = \frac{(1 + \sin \phi_{cv})}{(1 - \sin \phi_{cv})} \quad (3.2)$$

and the critical state angle of shearing resistance ϕ_{cv} is related approximately to bonding obliquity angle ϕ_o as

$$\sin \phi_{cv} = \left(\frac{\pi}{2} - \phi_o\right) \tan \phi_o \quad (3.3)$$

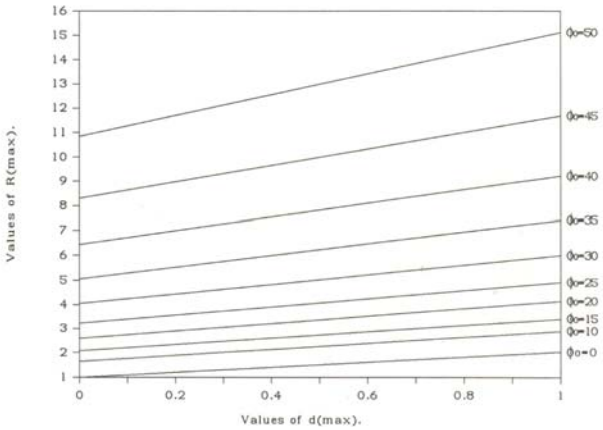

Figure 3.1 Chart for determining ϕ_o from triaxial compression tests

obtained from the result of an analysis of distributions of orientations of sliding contacts.

The minimum value of energy transmission ratio K_{min} is related to the bonding obliquity angle as

$$K_{min} = \frac{(1 + \sin \phi_o)}{(1 - \sin \phi_o)} \quad (3.4)$$

The maximum rate of dilation d_{max} is the maximum value of the rate of dilation $-dv/d\varepsilon_1$, where dv is the volumetric strain increment and $d\varepsilon_1$ is the strain increment in the direction of major principal stress σ_1'.Experiments show that R_{max} and D_{max} occur approximately simultaneously (see **Figures. 3.2** and **3.3**).

3. 1 To find ϕ_o numerically from triaxial compression tests

Equation 3.1 can be used to find ϕ_o from triaxial compression tests by the following algorithm that involves iteration:

1. Given: σ_1', σ_3' and d_{max} from a triaxial compression test.
2. Initialize ϕ_o = a value lower than the actual value.
3. $\sin \phi_{cvt} = \left(\frac{\pi}{2} - \phi_o\right) \tan \phi_o$
4. $K_{min} = (1 + \sin \phi_o) / (1 - \sin \phi_o)$
5. $K_{cvt} = (1 + \sin \phi_{cvt}) / (1 - \sin \phi_{cvt})$
6. $R_{max} = K_{cvt} + (2K_{min} - K_{cvt})d_{max}$
7. Compare calculated R_{max} with measured $R_{max} = (\sigma_1' / \sigma_3')_{max} = R_{max,m}$ the difference is

   $\Delta R_{max} = R_{max,m} - R_{max}$
8. n = the number of times ΔR changes signs, or 1, whichever is greater.
9. $\phi_o = \phi_o - (-1)^n / 10^{n-2}$
10. Return to step 3, until $\Delta R \leq$ tolerance.

3.2 Determination of dimensionless contact cohesion C_b

For constant values of ϕ_μ and C_b, **Equation 2.10** defines a linear relationship between tan ϕ_o and p_a / σ_n'. A series of triaxial compression tests may be conducted on a given material for a range of values of σ_3'.

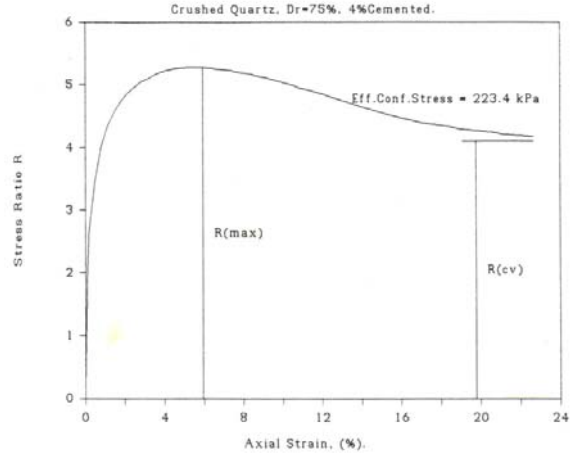

Figure 3.2 Typical stress-strain curve from a triaxial compression test

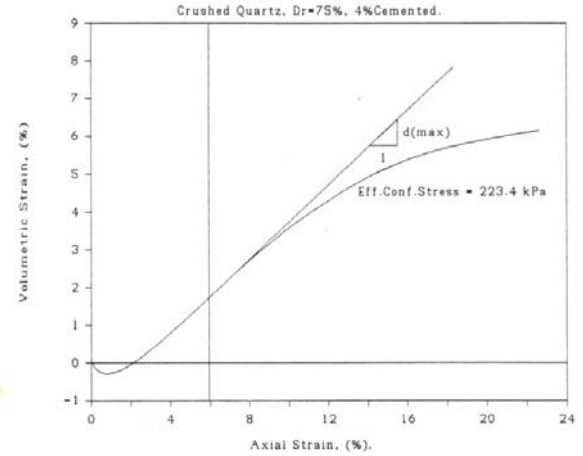

Figure 3.3 Typical volumetric strain vs. axial strain curve from a drained triaxial compression test

The measured values of R_{max} and d_{max} can be used to determine corresponding values of ϕ_o, and thus tan ϕ_o, from the algorithm described in the previous section, and σ_n' can be determined from **Equation 2.11** using ϕ_o, σ_3' and $\sigma_1' = R_{max}\,\sigma_3'$. The values of tan ϕ_o can then be plotted versus p_a / σ_n' to determine tan ϕ_μ and C_b from the intercept and slope respectively of a straight line approximating the data.

4. Consolidated Drained Triaxial Compression Tests

Theory has been developed in chapter 3 to determine the bonding obliquity angle ϕ_o and dimensionless contact cohesion C_b from the results of triaxial compression tests with volume change measurement.

In order to study dimensionless true cohesion $C_b = c_\mu / p_a$ in granular materials, 118 consolidated drained triaxial compression tests on specimens of cemented and uncemented sands were conducted. This chapter describes materials used for these tests, test results, and analysis.

Many variables relating to cement treated soils were held constant for this testing program. Quality of cement, environment during hydration, age of mixture at time of testing (curing time), mixing and compacting method, and the triaxial sample preparation procedure were the same for all samples.

4.1 Materials and test results

Ottawa sand and crushed quartz are the two materials tested. They were chosen to measure the effects of particle shape while holding the mineral type (quartz) constant.

Ottawa sand particles are very rounded, while crushed quartz particles are angular. Grain size basic properties are shown in **Table 4.1.**

Samples with two different densities were tested corresponding to relative density D_r = 25 percent and 75 percent for each material.

Cement content has a large effect on the strength of cemented soil, and it is assumed to have a large effect on dimensionless contact cohesion C_b. Because of the importance of this effect, four different cement contents were applied to the samples, namely 0, 2, 4, and 6 percents by dry weight.

Results of all consolidated drained triaxial compression tests are presented in this section. The minor principal effective stress σ_3', maximum stress ratio $R_{max} = (\sigma_1' / \sigma_3')_{max}$, and maximum rate of dilation d_{max} are obtained from stress strain curves for each test. Some sample curves are presented in **Figures 4.1** to **4.4** for Ottawa sand, and crushed quartz.

Table 4.1 Basic properties of ottawa sand and crushed quartz

Soil properties and symbols	Ottawa sand	Crushed quartz
particle shape	Rounded	angular
mineralogy	Quartz	Quartz
plasticity	NP	NP
specific gravity, G_s	2.67	2.64
min. void ratio e_{min}	0.507	0.654
max. void ratio e_{max}	0.713	0.986
diameter D_{50}	0.269	0.420
coeff. of uniformity C_u	3.086	1.840
coeff. of gradation C_c	0.974	0.947

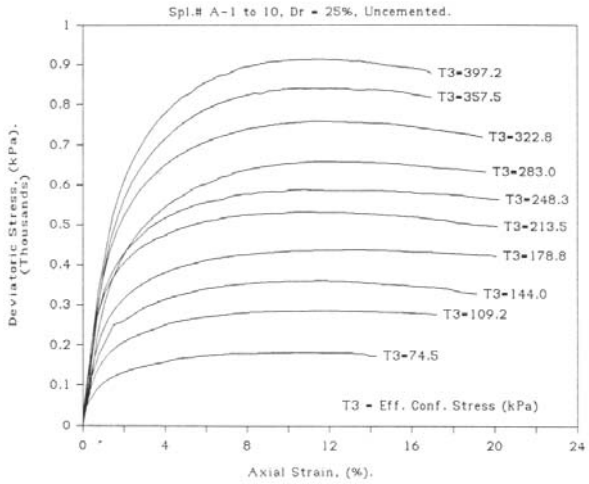

Figure 4.1 a. Deviatoric stress vs. axial strain; ottawa sand, dr = 25%, uncemented

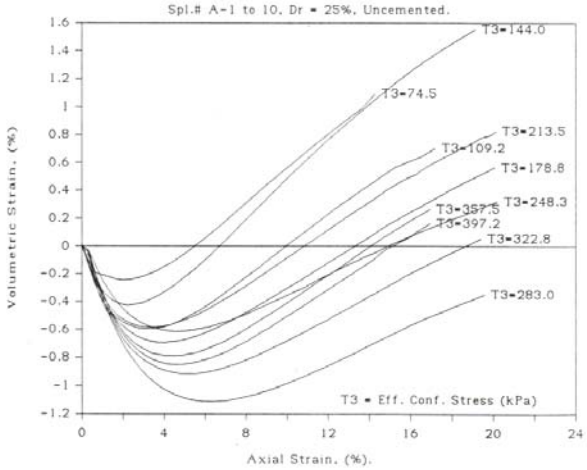

Figure 4.1 b. Volumetric strain vs. axial strain; ottawa sand, dr = 25%, uncemented

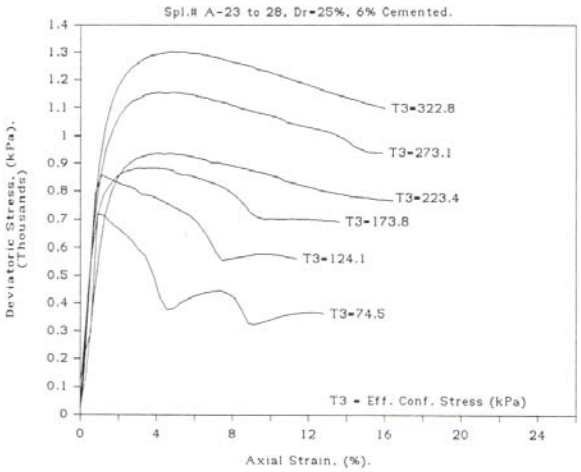

Figure 4.2 a. Deviatoric stress vs. axial strain; ottawa sand, dr = 25%, 6% cemented

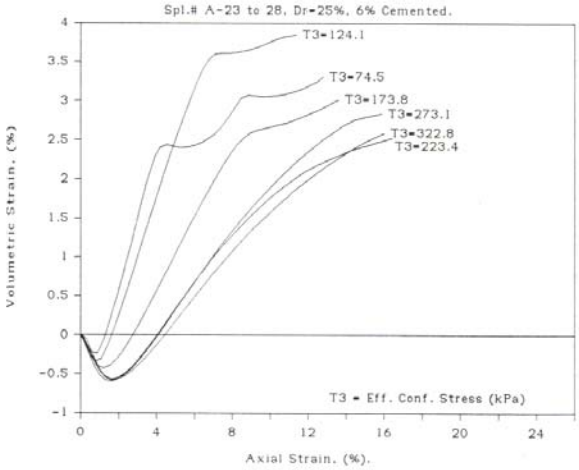

Figure 4.2 b. Volumetric strain vs. axial strain; ottawa sand, dr = 25%, 6% cemented

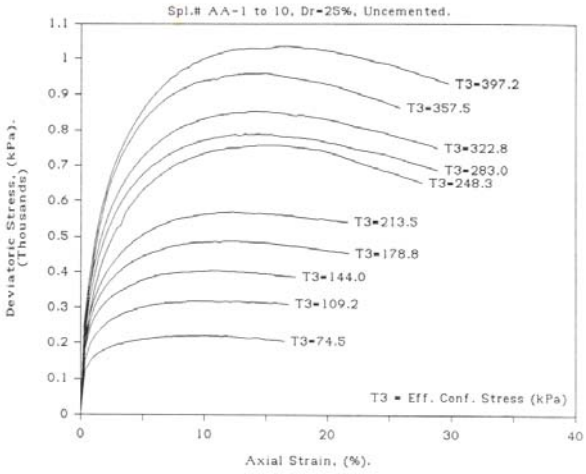

Figure 4.3 a. Deviatoric stress vs. axial strain; crushed quartz, dr = 25%, uncemented

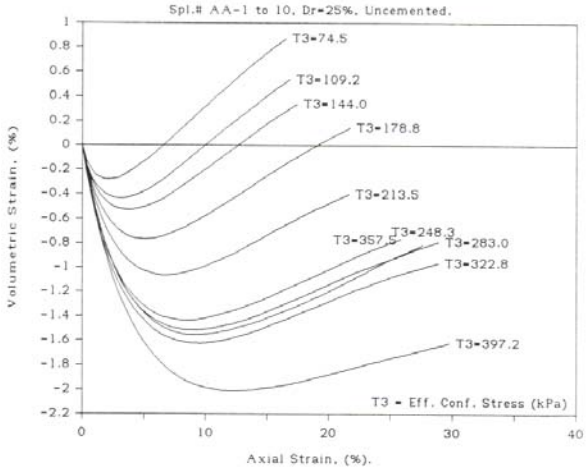

Figure 4.3 b. Volumetric strain vs. axial strain; crushed quartz, dr = 25%, uncemented

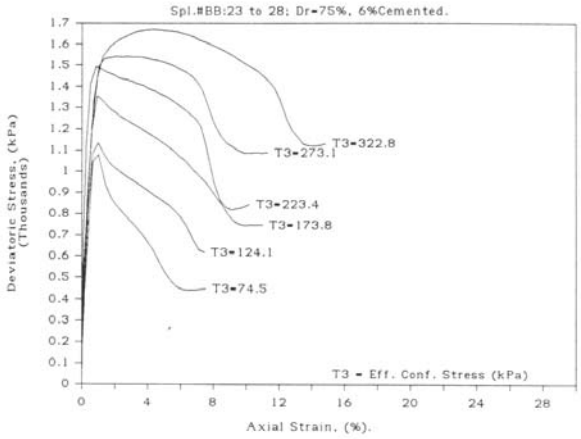

Figure 4.4 a. Deviatoric stress vs. axial strain; crushed quartz, dr = 75%, 6% cemented

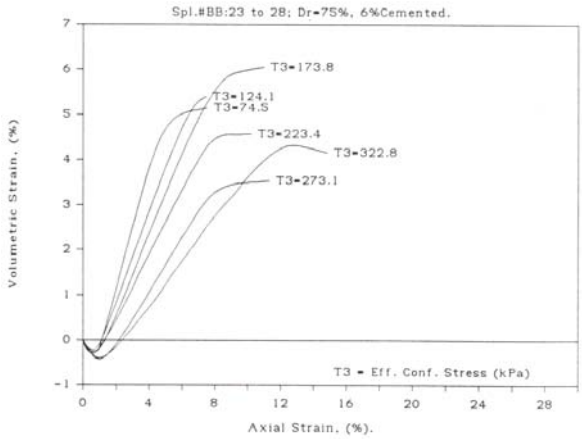

Figure 4.4 b. Volumetric strain vs. axial strain; crushed quartz, dr = 75%, 6% cemented

The maximum deviatoric stress $(\sigma_1' / \sigma_3')_{max}$, occurs approximately simultaneously with the maximum rate of dilation d_{max} on almost all samples (see chapter 3).

4.2 Dimensionless contact cohesion C_b

As stated in the last section of chapter 3, "Determination of Dimensionless Contact Cohesion," a linear relationship between the tan ϕ_o and p_a / σ_n' is assumed in order to define a constant value of dimensionless contact cohesion C_b. A line approximating each data set in **Figures 4.5** to **4.8** is found by linear regression where the tan ϕ_o intercept is constrained to the value for uncemented sand. The value of tan ϕ_o for uncemented sand is equal to tan ϕ_μ.

According to **Equation 2.9**, the slope of the line is equal to the dimensionless contact cohesion C_b, and the intercept is tan ϕ_μ. The values of C_b and tan ϕ_μ are shown in **Tables 4.2** along with the tan ϕ_o values defined by regression lines and the values of correlation coefficient R as a measure of how well a curve fits the data points. A curve fit with a value of correlation coefficient higher than 0.900 is a good fit, (Orvis, W. J.). A summary of C_b and tan ϕ_μ values is given in **Table 4.3** along with the corresponding R.

The determination of C_b as described above is based on the assumption that tan ϕ_μ is independent of confinement over a large stress range and thus is also independent of σ_n'. All four sets of results for uncemented sands, Ottawa sand and crushed quartz at relative densities 25 and 75 percents indicate that tan ϕ_μ is independent of σ_n', i.e. tan ϕ_o vs. p_a / σ_n' is approximately a horizontal straight line for each case with correlation coefficients above 0.900. Each horizontal line is assumed to define the constants tan ϕ_μ.

Other tables for the values of ϕ_o, sin ϕ_{cvt}, K_{min},, K_{cvt}, tan ϕ_o, p_a / σ_n', and results from regression tan ϕ_o, tan ϕ_μ, and C_b, for Ottawa sand, D_r = 75%, and for crushed quartz are not shown here, but the plotted data are shown in the following tables.

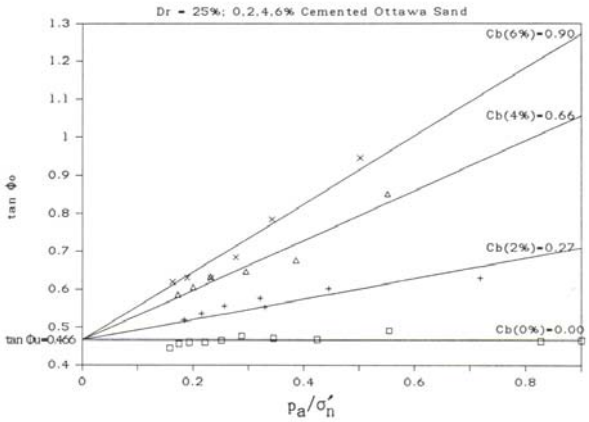

Figure 4.5 tan ϕ_o versus p_a / σ_n', Dr = 25%; 0,2,4,6% cemented Ottawa Sand

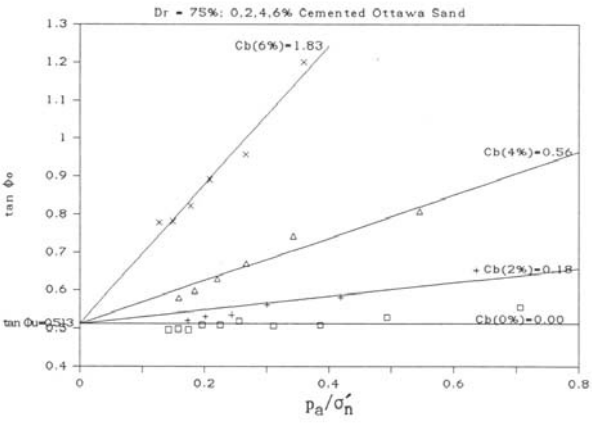

Figure 4.6 tan ϕ_o versus p_a / σ_n', D_r = 75%; 0,2,4,6% cemented Ottawa Sand

Table 4.2 $\phi_o, \sin\phi_{cvt}, K_{min}, K_{cvt}, \tan\phi_o, p_a / \sigma'_n$ and results from regression: $\tan\phi_o, \tan\phi_\mu$, and C_b, for Ottawa sand, D_r = 25%.

Spl. #	σ_3' (kPa)	ϕ_o	Sin $\phi_{\chi\sigma\tau}$	K_{min}	K_{cvt}	tan ϕ_o	P_a / σ_n'	tan ϕ_o from regrs.
Cement content = 0%								
A 1	74.5	24.88	0.53	2.453	3.230	0.464	0.827	0.466
A 2	109.2	26.14	0.55	2.575	3.415	0.491	0.555	0.466
A 3	144.0	25.08	0.53	2.471	3.258	0.468	0.424	0.466
A 4	178.8	25.22	0.53	2.484	3.277	0.471	0.346	0.466
A 5	213.5	25.44	0.54	2.506	3.311	0.476	0.288	0.466
A 6	248.3	24.95	0.53	2.459	3.239	0.465	0.251	0.466
A 7	283.0	24.71	0.52	2.437	3.205	0.460	0.222	0.466
A 8	322.8	24.68	0.52	2.434	3.201	0.460	0.194	0.466
A 9	357.5	24.52	0.52	2.419	3.178	0.456	0.175	0.466
A 10	397.2	23.98	0.51	2.369	3.103	0.445	0.158	0.466
From regression : tan ϕ_μ = *0.466, C_b = 0, R = 0.998*								
Cement content = 2%								
A 11	74.5	32.14	0.63	3.274	4.472	0.628	0.718	0.660
A 12	124.1	31.04	0.62	3.129	4.254	0.602	0.445	0.586
A 13	173.8	29.94	0.60	2.993	4.047	0.576	0.321	0.553
A 13R	173.8	28.95	0.59	2.876	3.871	0.553	0.330	0.555
A 14	223.4	29.09	0.59	2.892	3.895	0.556	0.257	0.535
A 15	273.1	28.20	0.58	2.791	3.743	0.536	0.215	0.524
A 16	322.8	27.42	0.57	2.707	3.615	0.519	0.184	0.515
From regression : tan ϕ_μ = *0.466, C_b = 0.27, R = 0.849*								
Cement content = 4%								
A 17	74.5	40.42	0.74	4.687	6.603	0.852	0.552	0.827
A 18	124.1	34.06	0.66	3.547	4.884	0.676	0.386	0.718
A 19	173.8	32.88	0.64	3.375	4.625	0.646	0.296	0.659
A 20	223.4	32.31	0.64	3.296	4.505	0.632	0.232	0.617
A 21	273.1	31.22	0.62	3.152	4.287	0.606	0.200	0.597
A 22	322.8	30.37	0.61	3.045	4.126	0.586	0.172	0.578
From regression : tan ϕ_μ = *0.466, C_b = 0.66, R = 0.968*								
Cement content = 6%								
A 23	74.5	43.38	0.77	5.388	7.657	0.945	0.503	0.916
A 24	124.1	38.10	0.71	4.223	5.904	0.784	0.343	0.773
A 25	173.8	34.36	0.66	3.591	4.950	0.684	0.277	0.714
A 26	223.4	32.15	0.63	3.275	4.473	0.628	0.232	0.674
A 27	273.1	32.20	0.64	3.282	4.484	0.630	0.189	0.635
A 28	322.8	31.72	0.63	3.218	4.387	0.618	0.163	0.612
From regression : tan ϕ_μ= *0.466, C_b = 0.90, R = 0.975*								

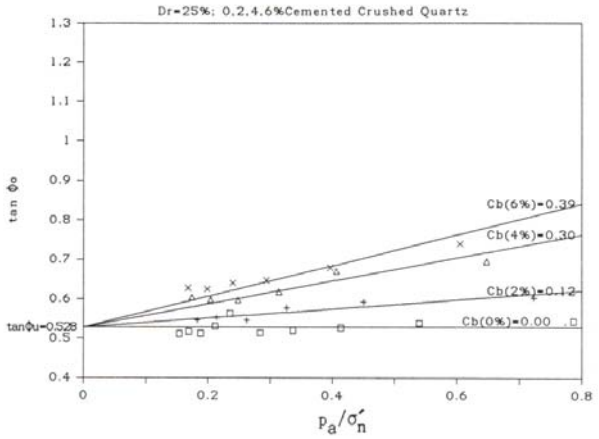

Figure 4.7 tan ϕ_o versus p_a / σ_n', D_r = 25%; 0,2,4,6% cemented Crushed Quartz

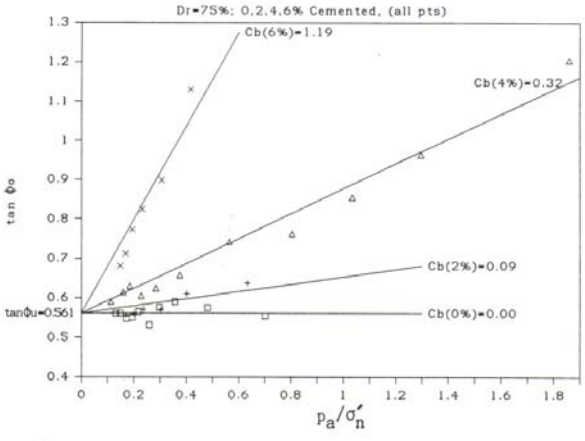

Figure 4.8 tan ϕ_o versus p_a / σ_n', D_r = 75%; 0,2,4,6% cemented Crushed Quartz (all points)

Table 4.3. Dimensionless contact cohesion C_b, tangent of contact friction angle tan ϕ_μ and the corresponding correlation coefficient R

Material	Relative density D_r (%)	Cement content (%)	C_b	tan ϕ_μ	Correlation coefficient R
Ottawa sand	25	0	0.00	0.466	0.998
		2	0.27	"	0.849
		4	0.66	"	0.967
		6	0.90	"	0.975
	75	0	0.00	0.513	0.994
		2	0.18	"	0.913
		4	0.56	"	0.967
		6	1.83	"	0.983
Crushed quartz	25	0	0.00	0.528	0.996
		2	0.12	"	0.913
		4	0.30	"	0.895
		6	0.39	"	0.864
	75 (all points)	0	0.00	0.561	0.995
		2	0.09	"	0.814
		4	0.32	"	0.988
		6	1.19	"	0.953
	75 (without B-23 B-33)	0	0.00	0.561	0.995
		2	0.09	"	0.814
		4	0.29	"	0.988
		6	1.06	"	0.957

Data for Ottawa sand with relative density equal to 25 percent in **Table 4.2** are plotted in **Figure 4.5**. Uncemented sand gives the value tan ϕ_μ = 0.466 (ϕ_μ = 25°) which is a reasonable value. Using tan ϕ_μ = 0.46 6, straight lines representing data points for 2, 4, and 6 percents cement, respectively, lead to values of C_b = 0.27, 0.66, and 0.90, with correlation coefficients R = 0.849, 0.967, and 0.975, (see **Table 4.3**). The value of C_b increases with increasing cement content.

Data for Ottawa sand with relative density equal to 75 percent are plotted in **Figure 4.6**. Uncemented sand gives tan ϕ_μ = 0.513 (ϕ_μ = 272°) which is reasonable for a higher density Ottawa sand, since ϕ_μ should increase with decreasing void ratio (Hardin 1985). Using tan ϕ_μ = 0.513, straight lines representing data points for 2, 4, and 6 percents cement, respectively, lead to values of C_b = 0.18, 0.56, and 1.83, with correlation coefficients R = 0.913, 0.967, and 0.983. The value of C_b increases with increasing cement content, and the increase is larger, compared with of C_b for relative density 25 percent.

Data for crushed quartz with relative density equal to 25 percent are plotted in **Figure 4.7.** Uncemented crushed quartz gives tan ϕ_μ = 0.528 (ϕ_μ = 27.8). Compared with Ottawa sand, crushed quartz particles are angular in shape, and the particle size is larger. Using tan ϕ_μ = 0.528, straight lines representing data points for 2, 4, and 6 percents cement, respectively lead to values of C_b = 0.12, 0.30, and 0.39 with correlation coefficients R = 0.913, 0.895, and 0.864 respectively.

The ϕ_μ = for crushed quartz can be compared to the value for Ottawa sand by using **Equation 4.5** (Hardin 1985). The Ottawa sand with D_r = 25 percent has initial void ratio e_i = 0.661; shape number n_s = 15 (rounded); D_{50} = 0.269 mm; and tan ϕ = 0.466 at the effective confining pressure σ_3' = 74.5 kPa. Based on results for several sands r_σ = 0.90 is used for Ottawa sand and r_σ = 0.75 for crushed quartz.

Substituting into **Equation 4.5** tan $\phi_{\mu std}$ is found = 0.556 is found. Using this $\phi_{\mu std}$ **Equation 4.5** can now be used to estimate ϕ_μ for crushed quartz with relative density D_r = 25 percent.

$$\tan\phi_\mu = \frac{7\tan\phi_{\mu std}}{(1+r_\sigma)(1+e_i)}\left[\frac{n_s}{25}\right]$$

$$\left[0.4+\frac{0.6}{1+6\dfrac{D_{50}}{D_{ref}}}\right]\left[r_\sigma+\frac{(1+r_\sigma)}{1+\dfrac{\sigma_3'}{10\,p_a}}\right] \qquad (4.5)$$

The following values are substituted, e_i = 0.903; D_{50} = 0.42 mm; n_s = 25 (angular); σ_3' = 74.5 kPa; and r_σ = 0.75. The computed value of tan ϕ_μ is 0.659 (ϕ_μ = 33.4°). This is considerably higher than indicated by the result in **Figure 4.7.** However, the effect of particle shape on values of ϕ_μ computed from **Equation 4.5** is large and the value n_s = 20 (sub-angular) gives = ϕ_μ = 27.8° as indicated by **Figure 4.7**.

Data for crushed quartz with relative density equal to 75 percent are plotted in **Figure 4.8**. Uncemented sand gives the value tan ϕ_μ = 0.651 (ϕ_μ = 29.3°). This tan ϕ_μ is larger than for crushed quartz with 25 percent relative density. Using the same procedure as crushed quartz with D_r = 25 percent in applying **Equation 4.5** for crushed quartz with D_r = 75 percent (e_i = 0.903), tan ϕ_μ = 0.722 is found for n_s = 25 and tan ϕ_μ = 0.578 for n_s = 20, which is very close to 0.561 found from regression in **Figure 4.8**.

Using tan ϕ_μ = 0.561, straight lines representing data points for 2, 4, and 6 percents cement, respectively, lead to values of C_b = 0.09, 0.29, and 1.06 with correlation coefficients R = 0.814, 0.988, and 0.957.

Using all available data (**Figure 4.8**), values of C_b are 0.09, 0.32, and 1.19 with correlation coefficients R = 0.814, 0.988, and 0.953 respectively.

The discarded data point, BB-33, is for tests with a very low effective confining pressure of 15 kPa. The increase of C_b with increasing cementation is larger than for crushed quartz with relative density equal to 25 percent.

5. Conclusions

Cohesive bonding at the sliding contacts in an element of soil has been studied using the model for soil strength proposed by Hardin (1985). That model contains two basic parameters, the bonding obliquity angle ϕ_o that represents both frictional and cohesive bonding at sliding contacts and the maximum rate of dilation d_{max} that represents kinematics of particle movement within an element of deforming soil.

According to the model tan ϕ_o is linearly related to the reciprocal of the effective stress normal to sliding contacts, σ_n'. The data presented in **Figure 4.5** indicate an approximately linear relationship. Furthermore, eleven tests over an extended stress range σ_3' = 15 to 480 kPa (**Figure 4.8**, 4% cement) were conducted to prove more conclusively the linearity of the relationship.

Also according to the model the slope of the linear relationship between tan ϕ_o and p_a / σ_n' defines the dimensionless contact cohesion C_b.

For Ottawa sand and crushed quartz with relative density 25 percent, C_b increases approximately linearly with cement content with very high correlation coefficients (0.996 and 0.994 respectively). $C_b = 0.152$ c for Ottawa sand with D_r = 25%, and $C_b = 0.067$ c for crushed quartz with D_r = 25%, where c is cement content.

For Ottawa sand and crushed quartz with relative density 75 percent, the relationships between C_b and cement content are nonlinear and are approximated by the relationship $C_b = \alpha c + \beta c^{\eta}$ where α, β and η are material constants. $C_b = 0.07c + 0.001c^{4.05}$ for Ottawa sand with D_r = 75% and $C_b = 0.03c + 0.001c^{3.781}$ for crushed quartz with D_r = 75%.

The value of C_b decreases with increasing relative density for 2 and 4 percents cement for both Ottawa sand and crushed quartz, but it rapidly increases with increasing density for 6 percent cement. A hypothesis to explain this is as follows. Both number of contacts and amount of cement increase with increasing density. However, the reduction of C_b with increasing density indicates that the increase in cement is not sufficient to provide the same bonding at the increased number of contacts for 2 and 4 percents cement.

The value of C_b for Ottawa sand (rounded material) is larger than that for crushed quartz (angular material) for all cement contents and for all relative densities.

The measured value of d_{max} which are plotted versus σ_3' for each cement content and for each material, are very close to the curves defined by **Equation 4.7** with the coefficients listed in **Table 4.5**. Values of d_{max} are higher for higher cement content, for all densities and for both materials, which means that the maximum rate of dilation increases with increasing cement content or with increasing contact cohesion, since contact cohesion increases with increasing cement content. Cemented sands behave like uncemented sands with higher density (Hardin, 1988).

Reference

Cauley, R.F., Kenedy, T.W., 1973, *"Proposal for Improved Tensile Strength of Cement Treated Materials"*, Highway Research Record No. 422, pp. 34-43.

Dupas, J.M., Pecker, A., 1979, *"Static and Dynamic Properties of Sand – Cement,"* Journal of Geotechnical Engineering Division, ASCE-GT3, pp. 419-436.

Gibson, R.E., 1953, *"Experimental Determination of the True Cohesion and True Angle of Internal Friction in Clays"*, Proceeding of the 3rd International Conference in Soil Mechanics, Zurich: vol. 1, pp 126-130.

Hardin, B.O., 1983, *"Advance Soil Mechanics Class Note"*, Department of Civil Engineering, University of Kentucky, Lexington, Kentucky.

Hardin, B.O., 1978, *"The Nature of Stress-Strain Behavior of Soils"*, Proceeding on Specialty Conference on Earthquake Engineering and Soil Dynamics, ASCE, Pasadena, California, June, pp. 19-21.

Hardin, B.O., 1985, *"Strength of Soils in Terms of Effective Stress"*, Richart Commemorative Lectures, GT Division Session, ASCE Fall Convention, Detroit, MI, October, pp. 1-78.

Hardin, B.O., 1988, *"The Low Stress Dilation Test"*, US Air force Office of Scientific Research.

Ho, K.H., 1971, *"Theoretical and Experimental Relationships between Stress Dilatancy and I.D.S. Strength Components"*, Ph.D. Dissertation, Department of Civil Engineering, University of Florida.

Ingles, O.G., Metcalf, J.B., 1972, *"Soil Stabilization Principles and Practice"*, Butterworths & Co. Publishing House, 1st edition, Melbourne.

Kezdi, A., 1979, *"Stabilized Earth Roads"*, Elsevier Scientific Publishing Company.

Kolias, S., Williams, R.I.T., 1984, *"Estimation of the Modulus of Elasticity of Cement Stabilized Materials"*, American Society for Testing and Materials.

Lambe, T.W., 1960, *"A Mechanistic Picture of Shear Strength in Clay"*, Research Conference on Shear Strength of Cohesive Soils, University of Colorado, Boulder, Colorado.

Lambe, T.W., Whitman, R.V., 1979, *"Soil Mechanics, SI version"*, John Wiley and Sons.

Mitchell, J.K., 1976, *"Fundamental of Soil Behavior"*, John Wiley and Sons.

Rad, N.S., 1983, *"Static and Dynamic Behavior of Cemented Sands"*, Ph.D. Dissertation, Stanford University.

Rad, N.S., Clough, G.W., 1984, *"New Procedure for Saturating Sand Cement Specimens"*, ASCE Geotechnical Eng.

Rowe, P.W., 1962, *"The Stress Dilatancy Relation for Static Equilibrium of an Assembly of Particles in Contacts"*, Proceeding of the Royal Society, London, Series A, vol. 269, no. 1339, pp. 500-527.

Schmertmann, J.H., Osterberg, J.O., 1960, *"An Experimental Study of the Development of Cohesion and Friction with Axial Strain in Saturated Cohesive Soils"*, Research Conference on Shear Strength of Cohesive Soils, Boulder, Colorado, pp. 643-694.

Schmertmann, J.H., 1971, *"The Shear Behavior of Soil with Constant Structure"*, Internal Report, Department of Civil Engineering, University of Florida.

Seed, H.B., 1976, *"Recent Development in Evaluating the Potential for Soil Liquefaction and Foundation Failure during Earthquake"*, Proceeding during Inaugural Symposium, September 17, pp. 61-115.

Sitar, N., 1979, *"Behavior of Slopes in Weakly Cemented Soils under Static and Dynamic Loading"*, Ph.D. Dissertation, Department of Civil Engineering, Stanford University, August.